Supporting Information

Polymer Carbon Nitride Nanosheets-Based Lamellar Membrane Inspired by "Couple Hardness with Softness" for Ultrafast Molecular Separation in Organic Solvent

Zhipeng Yan,[a] Liuqian Zhang,[a] Yudong Sang,[a] Dongyang Li,[a] Jingtao Wang,[a] Jing Wang,*[a] Yatao Zhang,*[a]

[a] School of Chemical Engineering, Zhengzhou University, Zhengzhou, Henan, 450001, People's Republic of China

* Corresponding author

E-mail addresses: wang.jing@zzu.edu.cn (J. Wang), zhangyatao@zzu.edu.cn (Y. Zhang)

EXPERIMENT PROCEDURES

Materials

The nylon substrate (pore size: 200 nm) was purchased from Tianjin Jinteng Factory. GO (thickness: 2-3 nm, size: 2–3 μm) utilized in this study was synthesized by a modified Hummers' method. Melamine and sodium chloride and all the other chemicals used were provided by Shanghai Chemical Reagent Co., Ltd. The dyes utilized in the nanofiltration experiment were acquired from Sigma-Aldrich (Shanghai, China) (Fig. S17). All reagents do not need to be further purified for use.

Synthesis of PCNN and b-PCNN

PCNNs were synthesized by reference to the relevant literature [1]. The procedure was as follows: 6 g of melamine and 30 g of sodium chloride were weighed and ground in an agate mortar to make a homogeneous mixture. Then, the synthesized mixture was heated to 650 °C for 2 h in a tube furnace with a nitrogen flow rate of 150 mL/min at 5 °C /min. After cooling to room temperature, the NaCl was removed by washing with deionized water several times, and then freeze-dried, and the resulting nanosheets were PCNN. The number of materials used in the synthesis of b-PCNN was the same as in the synthesis of PCNN, and the NaCl was first ball-milled in ethanol for one hour (520 rpm), followed by vacuum drying at 60 °C and then ground and mixed with melamine to make a homogeneous mixture. The next treatment was the same as in the preparation of PCNN.

Preparation of PCNN/GO Composite Membrane*s*

The preparation process of the PCNN/GO composite membrane is shown in Fig. 1b. 2.5 mg of PCNN was added to 200 mL deionized water (0.0125 mg/mL) and magnetic stirred (500 rpm) for

30 min, followed by ultrasonic treatment in an ultrasonic water bath (Dong Guan KSJ Co., PL-S80T, 40 Hz, rated power: 480 W) at 336 W for 30 min to ensure its homogeneous dispersion. 1 mg of GO was added to 100 mL of DI water with magnetic stirring for 30 min (500 rpm), followed by ultrasonic treatment in an ultrasonic water bath at 336 W for 30 min to prepare GO dispersion (0.01 mg/mL). Then, different volumes of GO dispersion (0.01 mg/mL) were mixed with 20 mL of PCNN dispersion (0.0125 mg/mL) at the mass ratio of 10/7.5/5/2.5:1. Afterward, the mixture was diluted to 200 mL and ultrasonicated again for 1 min (336 W). The mixed solution is then vacuum-filtered onto the nylon substrate membrane surface to prepare the PCNN/GO composite membrane. As shown in Fig. S1, the diameter of the bottom end of the filtration bottle used is 4 cm, and the effective area of the prepared composite membrane is 12.56 cm^2. The resulting membranes were dried at 80 °C for 5 mins and stored. The corresponding membranes were named PCNN/GO-10, PCNN/GO-7.5, PCNN/GO-5, and PCNN/GO-2.5. In addition, composite membranes containing only GO, PCNN, and b-PCNN were also prepared for experimental comparison.

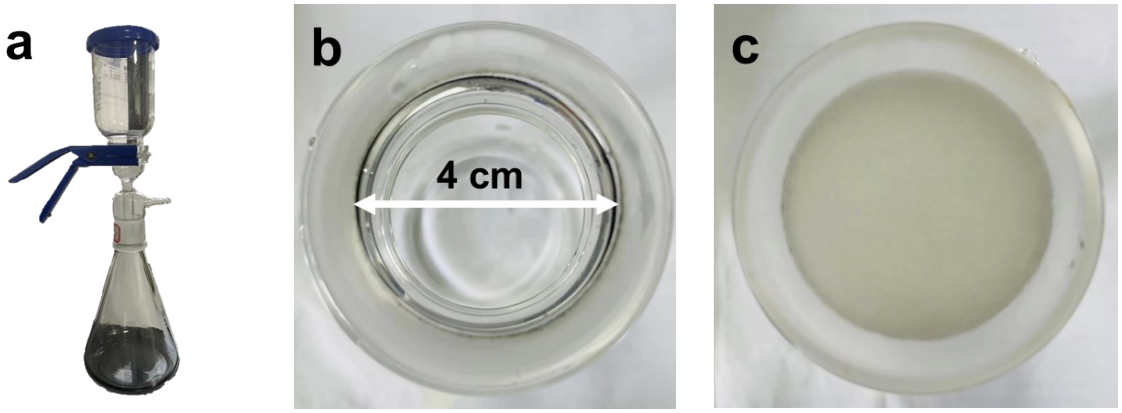

Fig. S1 (a) the filtration pumping apparatus used in membrane preparation. (b) Photograph of the bottom of the filter bottle, the diameter of the bottom end of the filtration bottle used is 4 cm. (c) Photograph of the sintered discs.

Permeance and Rejection Experiment

The nanofiltration performances (permeance and rejection) of the resultant membranes were measured by a homemade dead-end stainless-steel device (Fig. S2, test temperature: 25 ^{o}C). Long-term stability experiments were explored using a crossflow device (SF-SA, purchased from Hangzhou Saifei Membrane Separation Technology Co., Fig. S3). Before the performance test, membranes were pre-pressurized at 4 bar for 30 minutes to obtain stable permeance and rejection. To ensure the reliability of the data, at least five membranes prepared under the same conditions were used for the performance test. The data were recorded three times for each membrane, after that the test data of all membranes were analyzed and averaged.

The permeance (P; $L \cdot m^{-2} \cdot h^{-1} \cdot bar^{-1}$) of solvent was determined using Equation (1):

$$P = \frac{\Delta w}{\rho A \Delta p \Delta t} \quad (1)$$

in which Δw (kg) refers to the permeance weight of solvent; ρ (kg/L) refers to the density of solvent; A (m^2) refers to the effective area of the device (Dead-end device: 3.14 cm^2, cross flow device: 7.065 cm^2); Δp (bar) refers to the test pressure (1 bar); Δt (h) refers to the test time.

The rejection rate (R; %) was calculated via Equation (2):

$$R = (1 - C_p/C_f) \times 100\% \quad (2)$$

in which C_p and C_f refers to the concentrations of the permeate and feed solutions, respectively. The dye was dispersed in ethanol (0.02 g/L) as feed solution (in all rejection experiments), and its concentration was tested by a UV–vis spectrophotometer (SHIMADZU, UV-1800). Static

adsorption experiments were conducted to exclude the effect of membrane adsorption in Fig. S15.

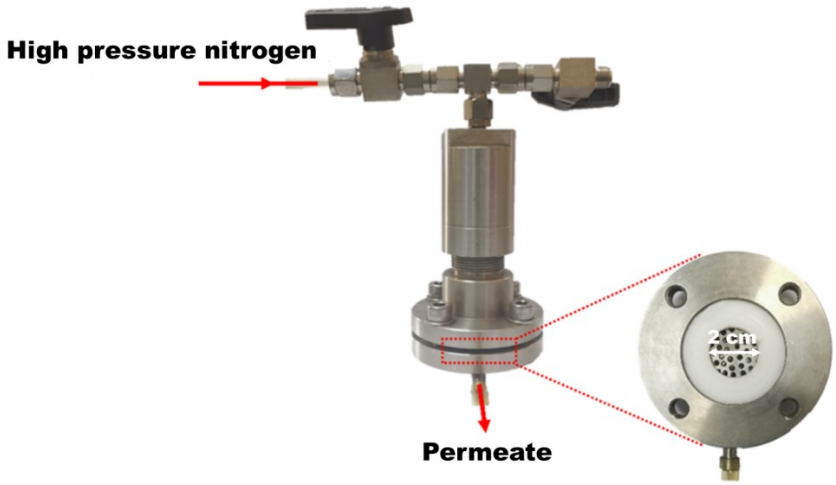

Fig. S2 The homemade dead-end device for the performance measurement of the membranes.

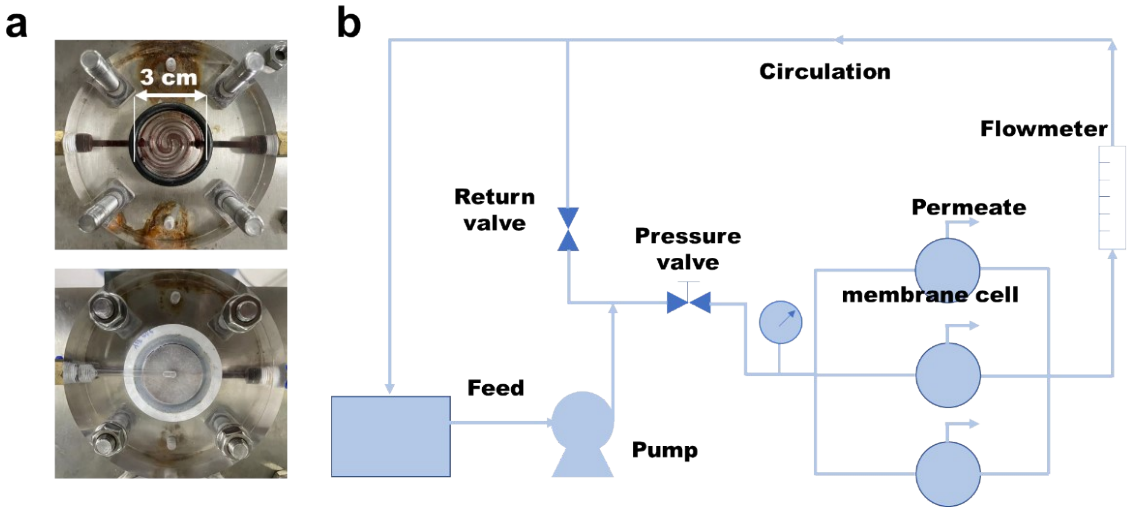

Fig. S3 Photographs of (a) the membrane cell in the crossflow device for the long-term stability test (the diameter of the membrane cell used is 3cm) and (b) the pipeline schematic.

Computational Details

The COMPASS force field was employed to model PCNN, GO, and methanol molecules. The single-layered PCNN and GO were built with sizes of 26.848 Å (y) × 22.438 Å (z) and 29.119 Å (y)

×23.196 Å (z), respectively. The single-layered PCNN contained 85 C atoms, 110 N atoms 30 H atoms, and 30 Na ions, while the single-layered GO contained 251 C atoms, 98 O atoms, and 41 H atoms. The unsaturated C atom from PCNN and GO was terminated by an H atom. All channel size is set to be 1.07 nm, corresponding to the one approximately calculated in our experiments for PCNN. The GO and PCNN nanosheets lay in parallel to the YZ plane. 300 methanol molecules were added to each system. All modeling and molecular dynamics (MD) simulations were implemented in BIOVIA Material Studio [BIOVIA Material Studio 2019 (19.1.0.2353)]. The nanosheet is geometrically optimized before MD simulation and becomes to be fixed during the NVT simulation procedure. The smart method is used in the energy minimization process. The overall simulation time is 10 ns, including 7 ns of equilibration and 3ns of production, where the last 3 ns are used for post-analyses. The steady state of the velocity distribution perpendicular to the YZ plane with time can be observed in Fig. S19. The Berendsen thermostat was employed to regulate the temperature. The cutoff distance for van der Waals interactions was 15.5 nm, with a long-range dispersion correction applied for energy.

Characterization

The micromorphology of PCNN, b-PCNN powders, and membranes were characterized by a scanning electron microscope (Zeiss/Auriga-bu) at 5.0 kV, transmission electronic microscopy (TEM; Thermo Fisher Scientific, Talos F200S), and Bruker Dimension FastScan AFM device. The X-ray diffractions (XRD, PANalytical Empyrean) of GO, PCNN, b-PCNN powders, and different membranes were characterized at 5°-60° by Cu-Kα radiation. The chemical structures of GO, PCNN, and b-PCNN powders were measured through attenuated total reflection Fourier transform infrared (FT-IR, Thermo Fisher Scientific Nicolet 7600). The element compositions of

PCNN powders were tested by XPS (PHI 5000 Versaprobe) with Kα radiation. Particle size analyses used a laser particle sizer (Micromeritics Instrument Co., NanoPlus-3). PCNN, GO, and PCNN/GO composites were characterized by Raman spectroscopy in a 532 nm excitation wavelength (Horiba LabRAM HR Evolution). Nanoindentation tests were applied to study the mechanical stability and contact hardness and elastic modulus at the nanoscale of the laminate membrane by NANOVEA PB1000 Hardness Tester. The detailed test method is as follows: the membrane is cut to the size of 1cm*1cm and pasted on a special metal module. The load force was set to 0.5 mN in the software subsequently the nanoindentation test was performed and the load-depth curve was obtained. Mechanical parameters were calculated by analytical software using the Oliver-pharr modeling analysis.

RESULTS AND DISCUSSION

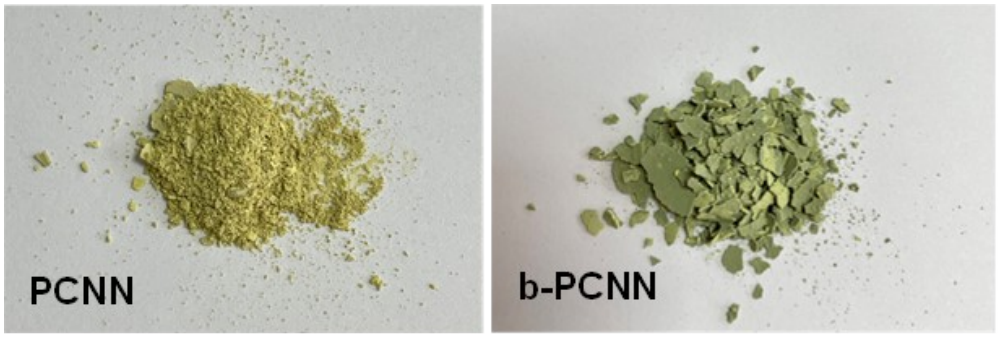

Fig. S4 The PCNN powder prepared by grinding NaCl shows a light yellow color, while the b-PCNN prepared by ball-milling NaCl exhibits a matcha-green color.

As Fig. S3a shows, the XRD diffraction of synthesized GO sheets exhibits a sharp characteristic peak, which is in agreement with the literature.[2] Fig. S3b shows the FT-IR spectrum of GO. There

is a strong broad peak at around 3407 cm^{-1} corresponding to the -OH moiety on GO, and the peak at 1725 cm^{-1} indicates the characteristic absorption peak of C=O.[3] TEM images showed that the prepared GO possessed large dimensions with distinct fold-like undulations on the surface (Fig. S6a). Particle size distribution and AFM images showed that the lateral size of the graphene oxide flakes was about 2-3 µm and the thickness was about 2-3 nm (Fig. S6b and S7a).

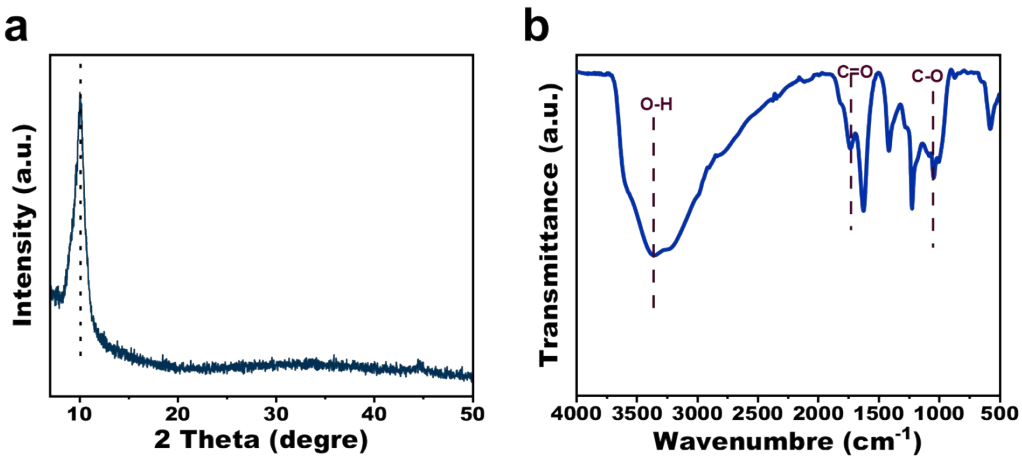

Fig. S5 (a) XRD of GO powder. (b) FT-IR spectrum of GO powder.

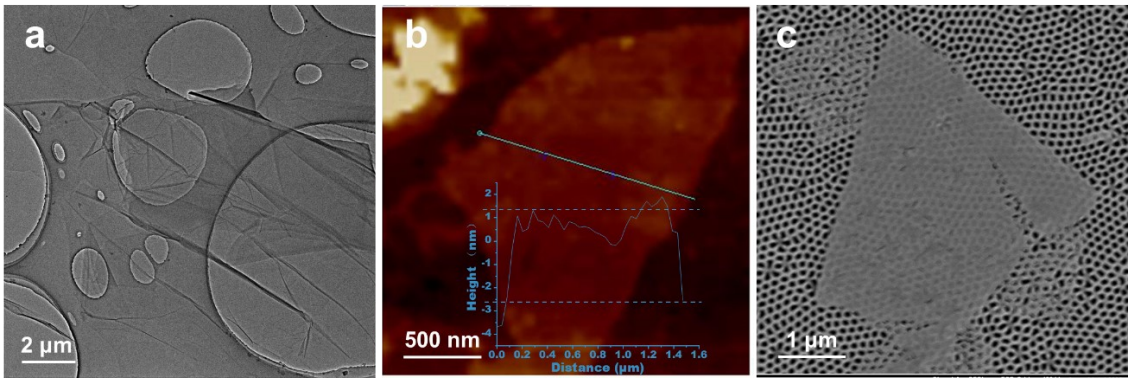

Fig. S6 (a) TEM image of GO. (b) AFM image of the prepared GO nanosheets, the inset figure displays the height profile of the blue line traced on the AFM image. (c) the SEM images of GO.

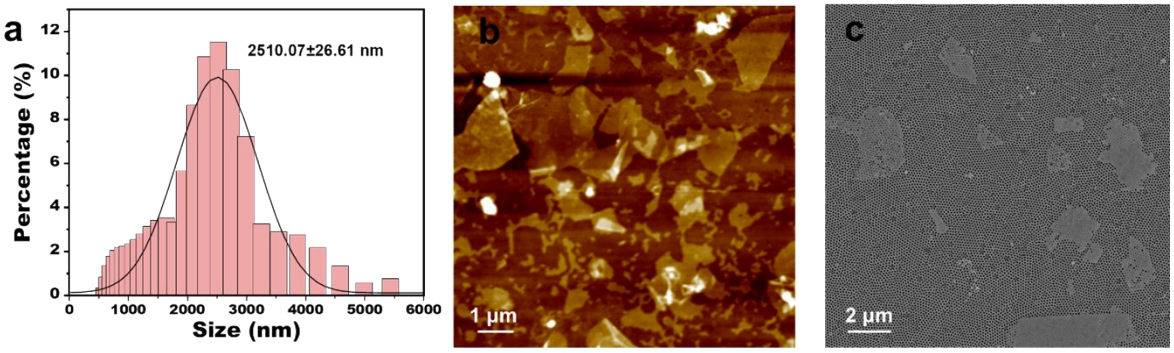

Fig. S7 (a) Particle size distribution of GO nanosheets obtained by laser particle sizer. (b) AFM image of GO nanosheet distribution. (c) SEM image of GO nanosheet captured at 5000x.

The dispersity of PCNN in water is excellent and no significant precipitation was observed even after 20 days of resting (Fig. S8).

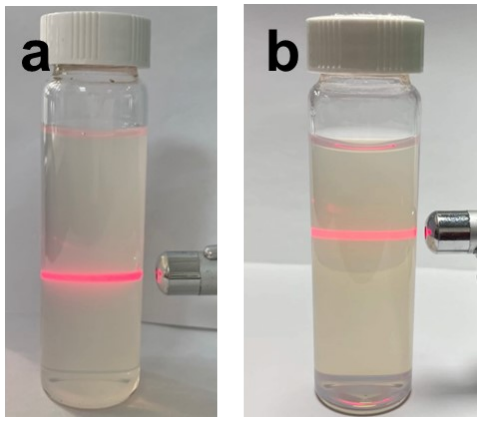

Fig. S8 Tyndall effect of PCNNs dispersed in water for (a) 0 days and (b) 20 days.

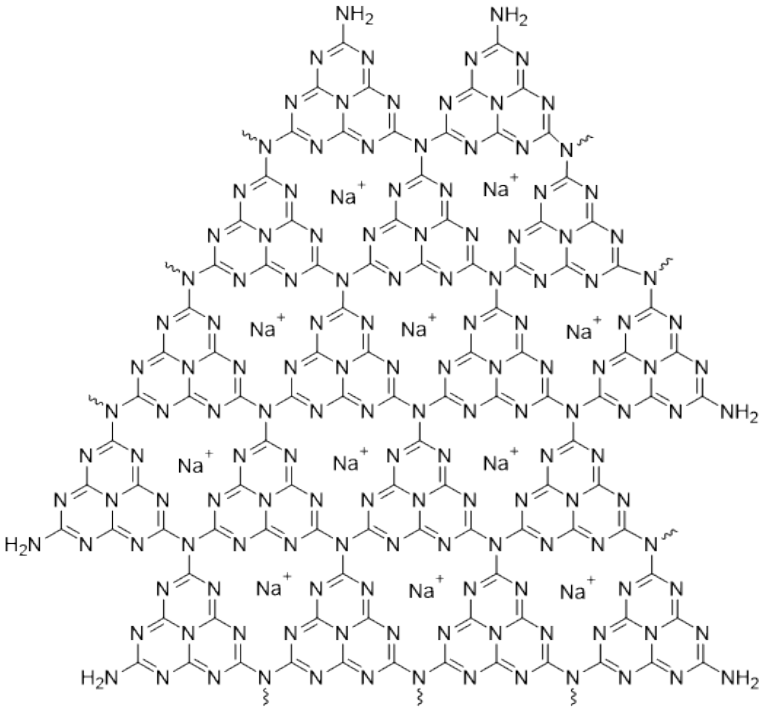

Fig. S9 The structural formula of PCNN.

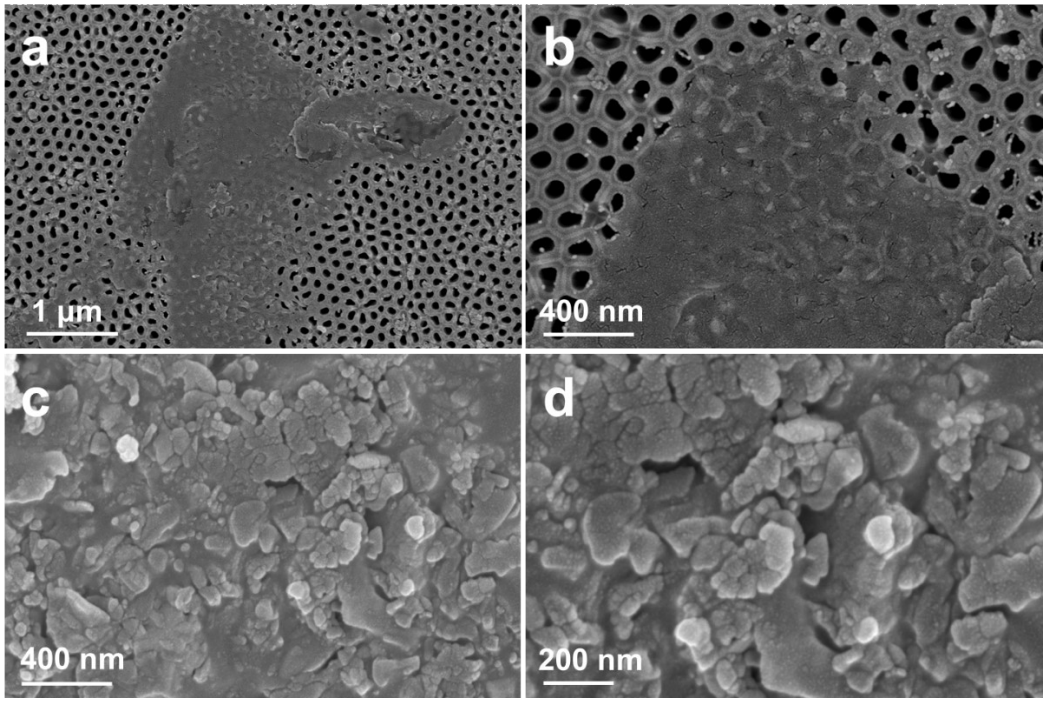

Fig. S10 SEM images of (a, b) PCNN and (c, d) b-PCNN powder.

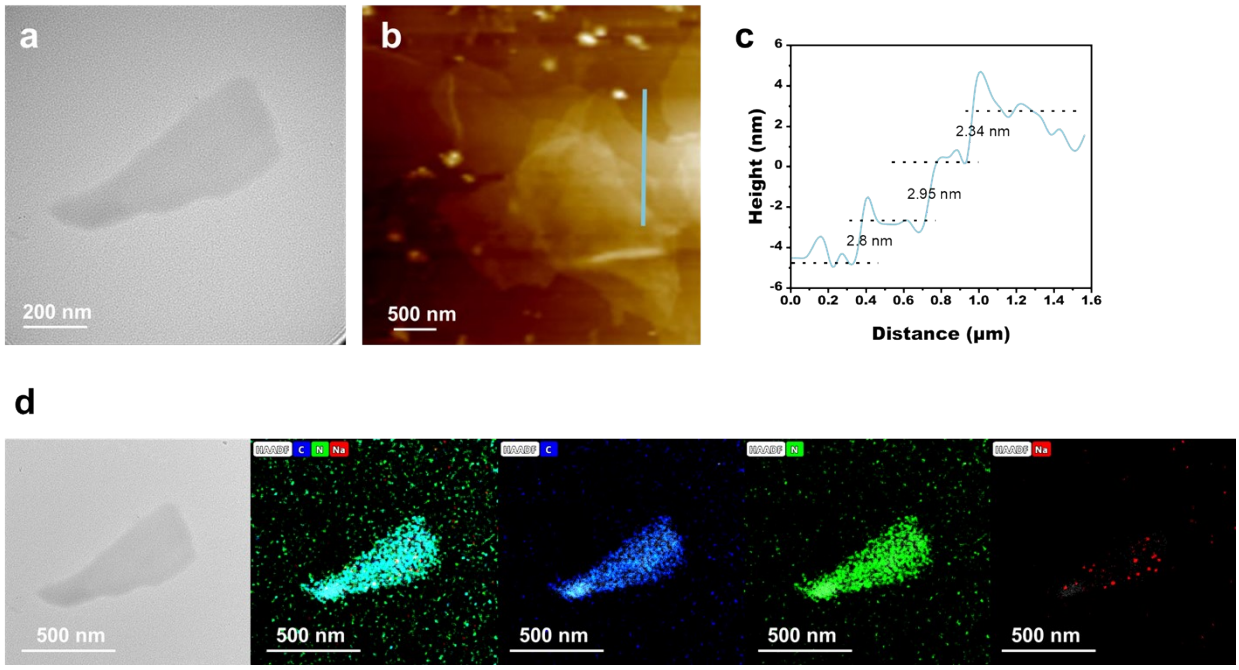

Fig. S11 (a) TEM images of PCNN and (b) AFM images of PCNN. (c) Analysis of the thickness of the drawn portion of (b) shows that the PCNN in a single layer is only 2-3 nm. (d) The EDS elemental mapping images of PCNN.

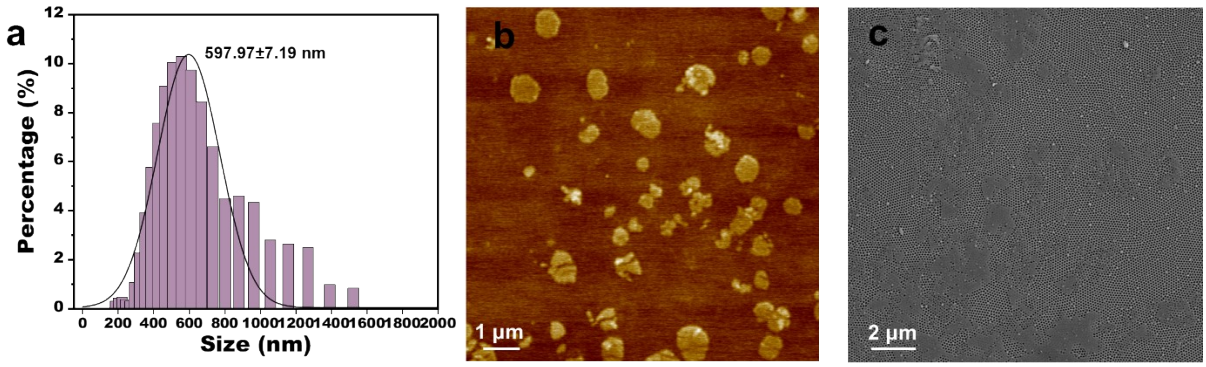

Fig. S12 (a) Particle size distribution of PCNN obtained by laser particle sizer. (b) AFM image of PCNN distribution. (c) SEM image of PCNN captured at 5000x.

Fig. S13 shows the Raman spectra of PCNN, GO, and PCNN/GO composites. The peaks at 731cm^{-1} correspond to the heptazine ring breathing mode and 1235 cm^{-1} attributed to the stretching vibration mode of C–N heterocycles.[4, 5] The weaker peak intensity of PCNN in the D-band (lattice

defects) indicates the low degree defects of PCNN [6]. The intensity ratio of the G-band (degree of graphitization) to the D-band (I_G/I_D) in GO is 1.04, suggesting that the synthesized GO has relatively complete lamellae sheets.[7]

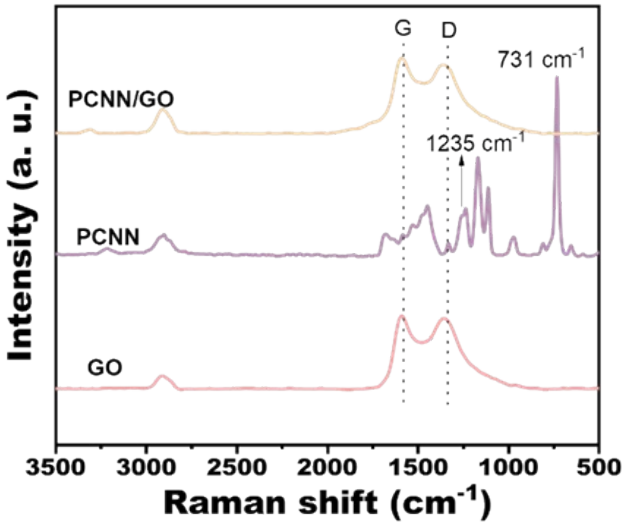

Fig. S13 Raman spectra of PCNN, GO, PCNN/GO composite. (Characterization using a 532 nm laser wavelength.)

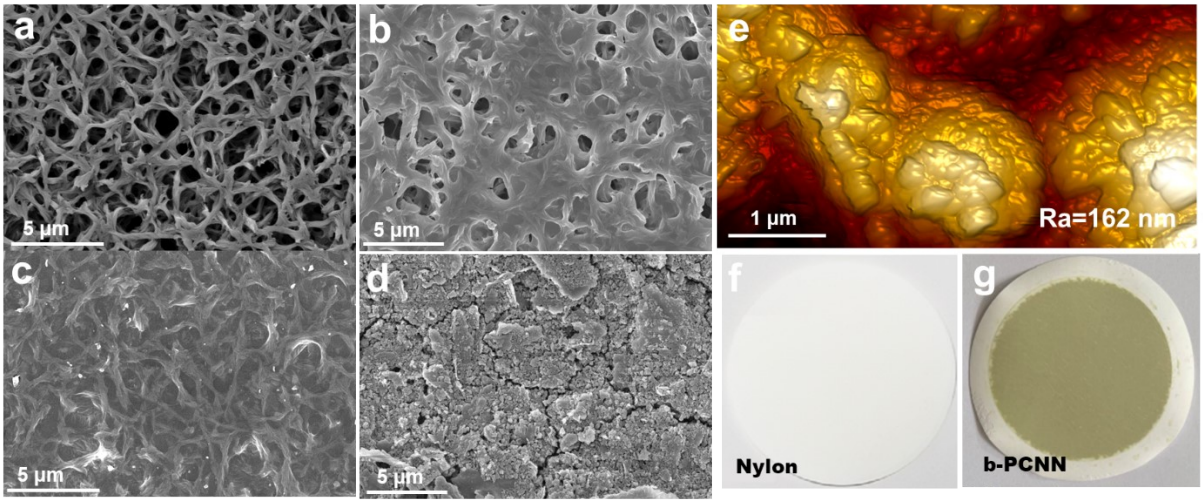

Fig. S14 SEM images of (a) Nylon membrane, (b) GO-0.05 membrane (loading amount: 0.05 mg GO), (c) GO-0.1 membrane (loading amount: 0.1 mg GO), (d) b-PCNN-3 membrane(loading amount: 0.3 mg GO). (e) AFM images of b-PCNN-3. Photos of (f) Nylon substrate membrane and (g) b-PCNN-3 membrane (loading amount: 3 mg b-PCNN).

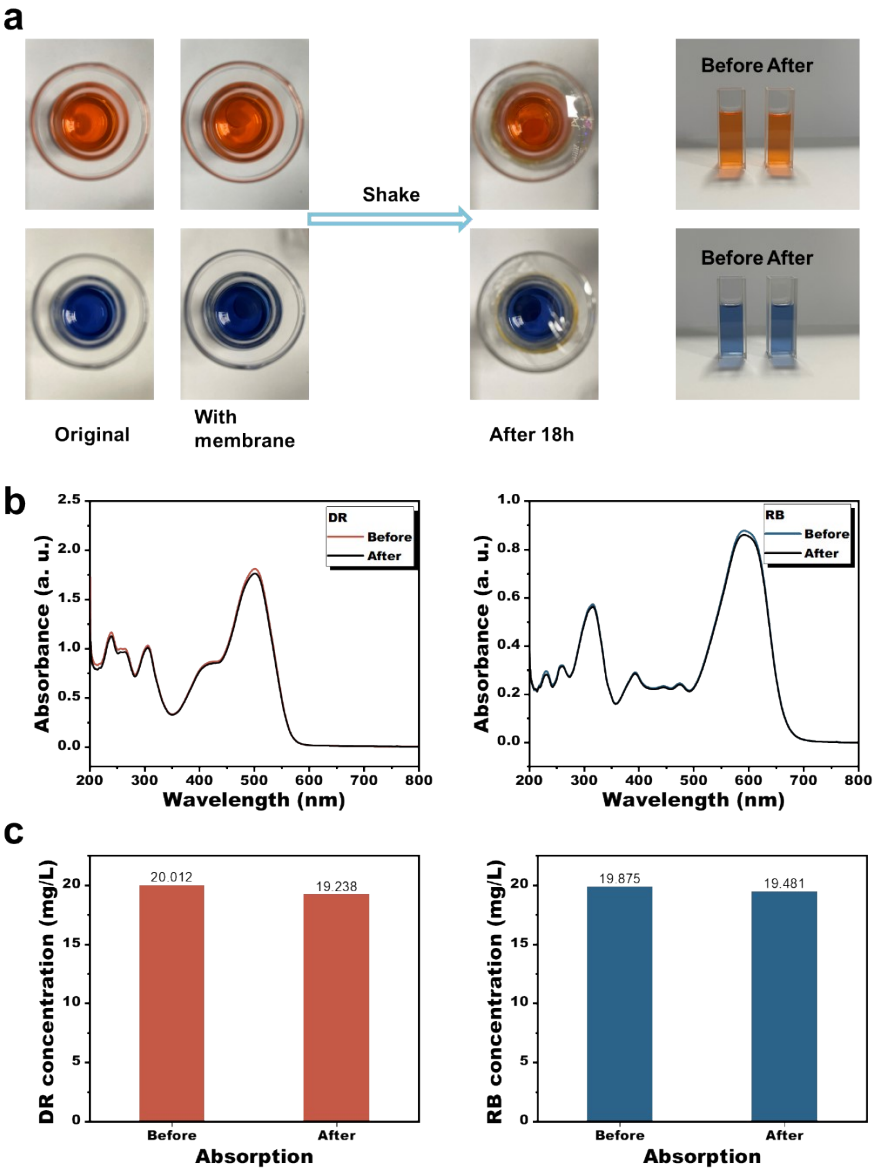

Fig. S15 (a) Static adsorption test procedure of dyes by membranes. UV spectrum of solution before and after adsorption test for (b) DR and RB. (c) Concentration changes in RB and DR. The

membrane was immersed in a solution of 20 mg/L of RB and DR (30 mL) and shaken in a constant temperature incubator shaker at 30 °C, 170 rpm for 18 hours (Taicang Huaying, HZQ-F100).

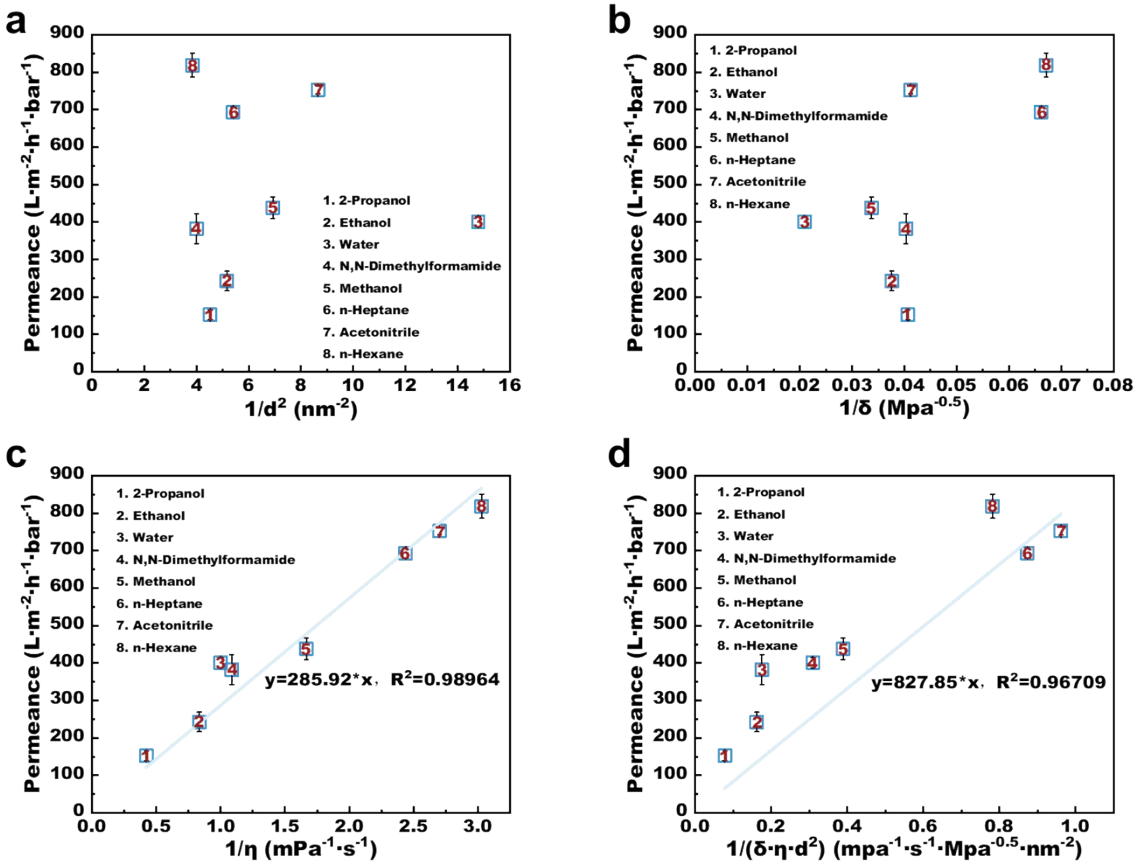

Fig. S16 The scatter plot between the inverse of the square of (a) the solvent kinetic diameter (d^{-2}) and (b) the inverse of the total Hansen solubility parameter (δ^{-1}) with the pure solvent permeance in PCNN/GO membranes (loading: 0.25 mg PCNN, 0.05 mg GO). No clear linear relationship in (a) and (b). Pure solvent permeance as a function of (c) the inverse of the viscosity (η^{-1}) and (d) the multiparameter ($\delta^{-1}\cdot\eta^{-1}\cdot d^{-2}$) for PCNN/GO membranes. The blue line indicates the fitted linear relationship. Solvents used included 2-propanol, ethanol, deionized water, N, N-dimethylformamide (DMF), methanol, n-heptane, acetonitrile, and n-hexane. Tested at 25 °C and 1 bar pressure.

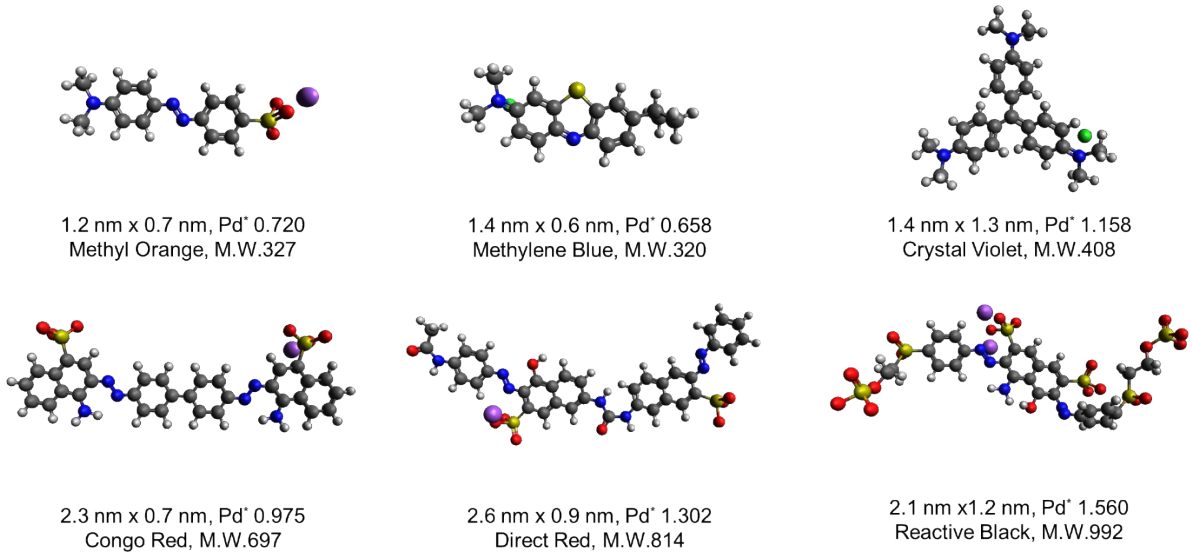

Fig. S17 Six dye molecules with different sizes were tested in the separation performance test. The molecular sizes were simulated and estimated, using the Molecular Mechanics 2 method in the Chem3D software. The permeable molecular diameter (Pd*) was estimated based on the energy-minimized molecular structures visualized with the Avogadro molecule editor and visualizer (https://avogadro.cc/) using the space-filling model. The Pd* was manually measured for the molecules by drawing a circle circumscribing the smallest projection of the molecular structure using ImageJ.

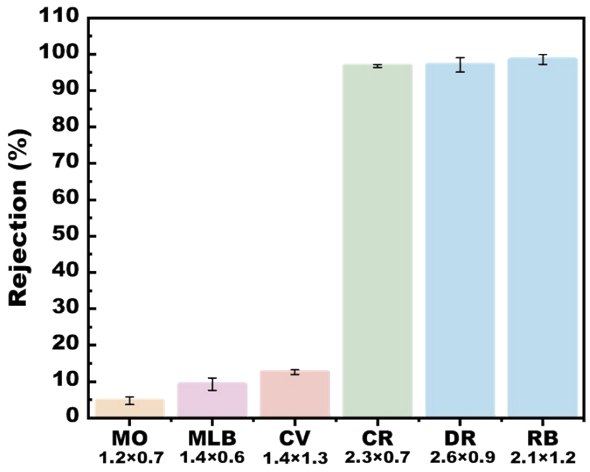

Fig. S18 Dye rejection of the PCNN/GO membrane. The dyes utilized included methyl orange (MO), methylene blue (MLB), crystal violet (CV), Congo red (CR), direct red (DR), and reactive black (RB). The relevant sizes (nm) are noted below their abridgments. (Measurement condition: 0.02 g/L dye in methanol; pressure: 1 bar).

The simulation is 10 ns from the beginning of this time, with the first 7 ns as the equilibration period and the last 3 ns as the production period used for post-analyses. As can be seen from Fig. S19 below, when time is over 7 ns, in addition to a dynamically stable density and energy, the velocity distribution perpendicular to the YZ plane shows a steady-state as well.

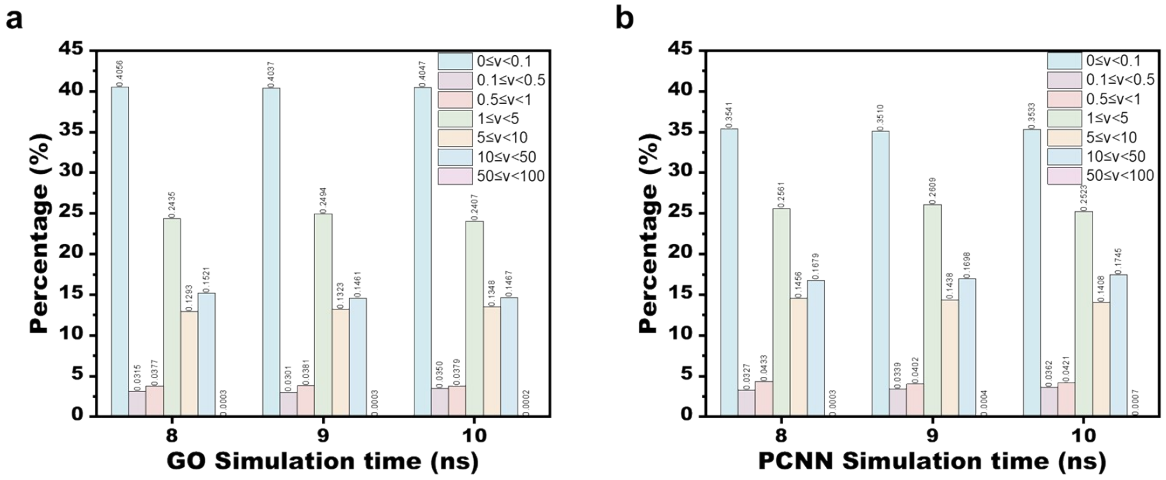

Fig. S19 Statistical percentages of velocity distributions of (a) GO and (b) PCNN for different simulation timescales

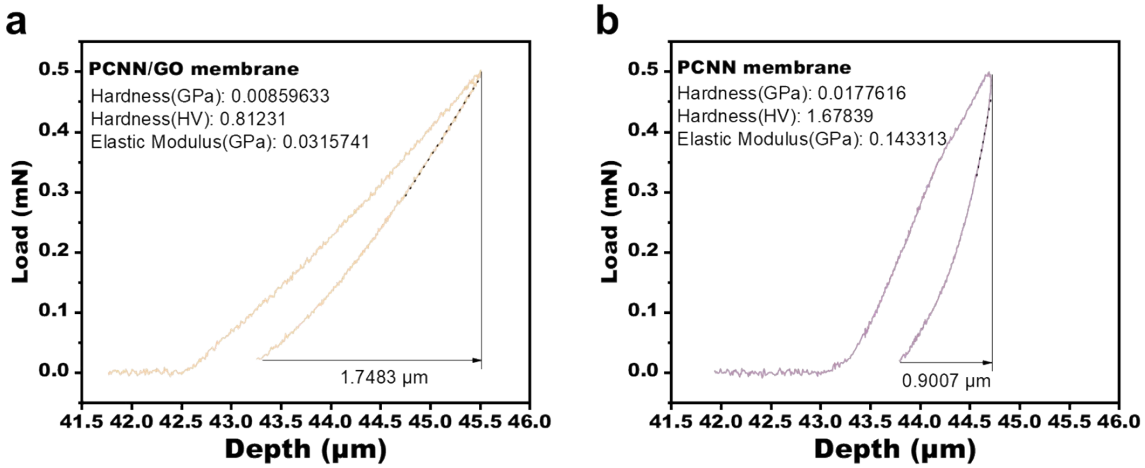

Fig. S20 Load-depth curves obtained from nanoindentation testing of (a) PCNN/GO membrane and (b) PCNN membrane, where the black dotted line indicates the linear part used by the software to calculate the mechanical parameters.

To further explore the positive effect of the interaction between the GO and PCNN on the membrane, nitrogen bubbling experiments, and ultrasonic oscillation experiments were also performed to verify the stability of the PCNN/GO membrane compared to the PCNN membrane (Fig. S21, solvent volume: 30 mL). After a 5-minute nitrogen bubble test, it was found that the PCNN membrane showed that the material was falling off, and the surface color of the membrane began to lighten, exposing the substrate membrane. The comparative PCNN/GO membrane, on the other hand, maintained a more intact appearance (Fig. S21d). In a three-minute sonication experiment on the membranes (336 W), the PCNN/GO membranes maintained good morphology in all three solvents, and there was no significant Tyndall effect present using laser irradiation of the liquid (Fig. S22). In contrast, the PCNN membrane experienced material detachment after sonication, accompanied by the presence of a clear Tyndall effect.

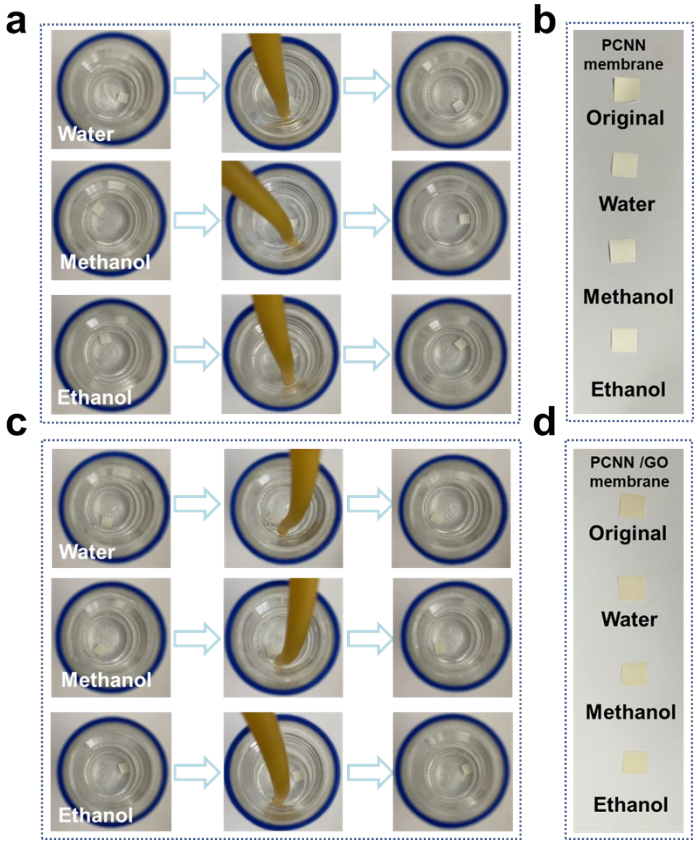

Fig. S21 Nitrogen bubbling experiments were performed on (a) PCNN membranes and (c) PCNN/GO membranes. (b) PCNN membrane and (d) PCNN/GO membrane were compared with the original membranes after removal from the test.

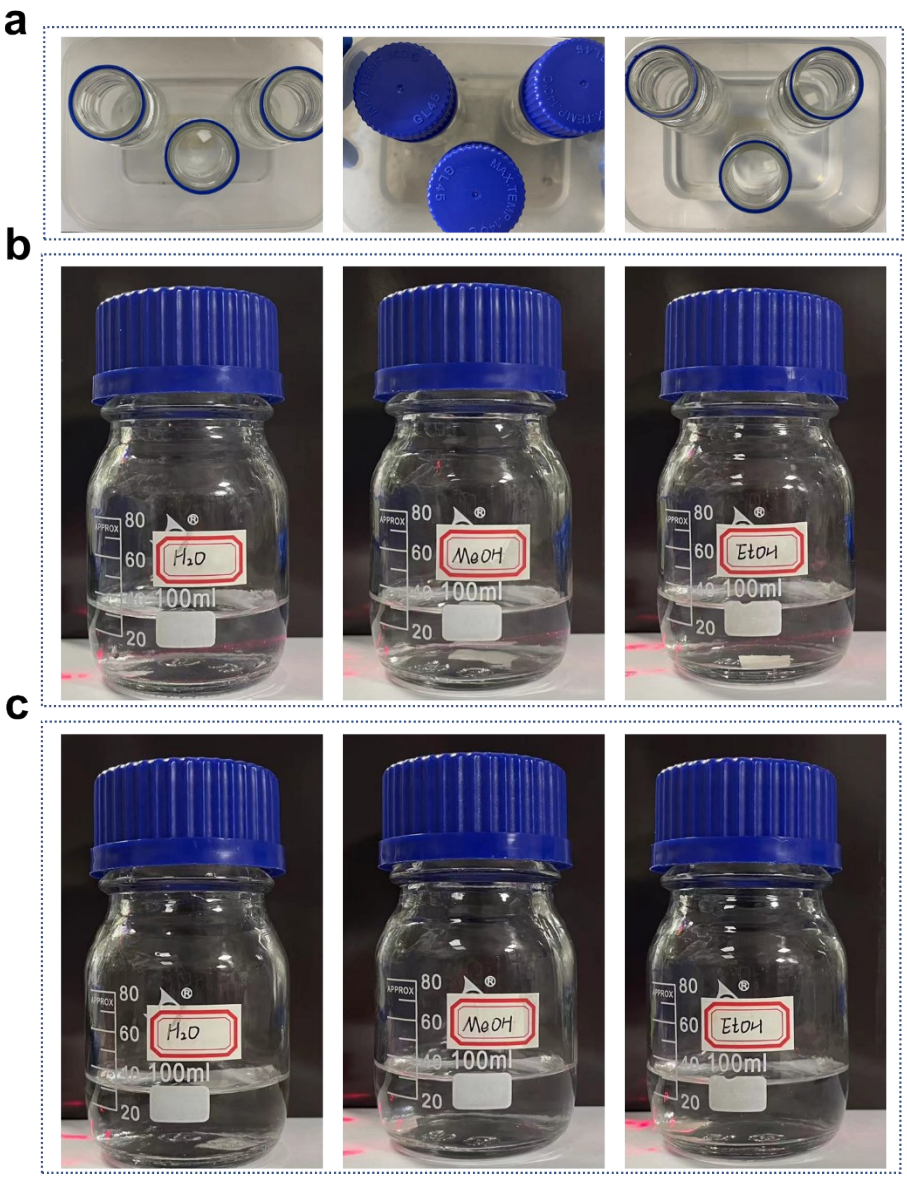

Fig. S22 (a) Membranes for water bath sonication experiments in three solvents. Laser irradiation of solvents containing (b) PCNN membrane and (c) PCNN/GO membrane after experiments, respectively. PCNN membranes showed the Tyndall effect in all three solvents.

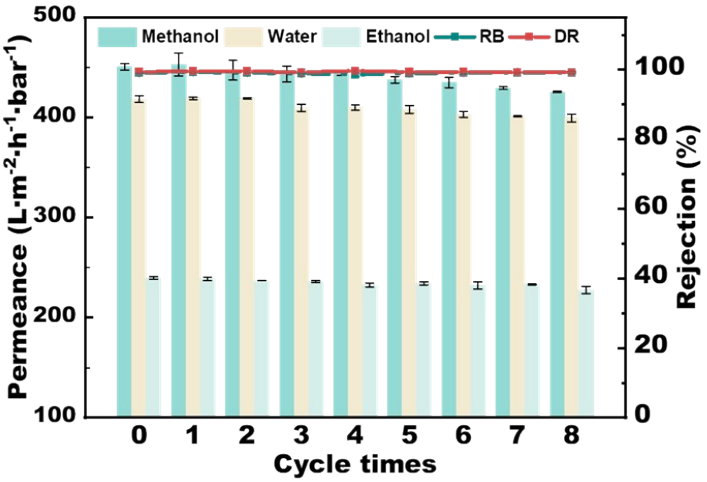

Fig. S23 Membrane reusability performance. After each experiment, the membrane surface was rinsed three times using pure ethanol solvent and then permeated with 30 ml of pure ethanol for a total of three times. The membranes were then tested again for permeance and rejection.

As shown in Fig. S24, it can be seen that the PCNN/GO membrane also maintains a certain chemical stability by immersion in acid and alkali solution after 24h.

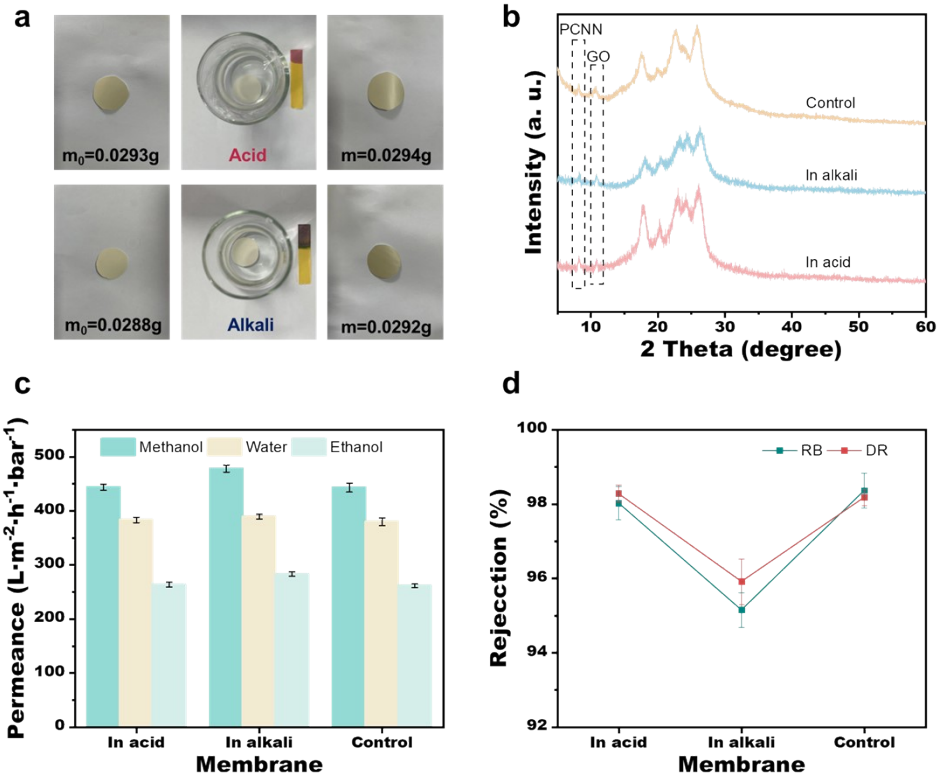

Fig. S24. (a) Acid and alkali immersion processes in membranes (0.1 mol/L). (b) XRD spectra of membranes after 24h immersion in acid and alkali. Changes in (c) permeance and (d) rejection after immersion in acids and alkalis. The control group was left untreated for 24 hours.

Table S1 Mechanical parameters of some common nanosheet materials.

Materials	Theoretical Young's modulus (Gpa)	Mohs hardness
GO	100 ~ 300	< 1
rGO	100 ~ 400	< 1
BN	340～350	0.47
2D MOF	< 100	\

2D COF	1 ~ 100	\
MoS_2	200 ~ 400	1~1.2
MXene	< 400	\
CN	> 900	9~10

Table S2 Solvent parameters. viscosity, polarity, kinetic diameter, and total Hansen solubility parameter of the solvents used in this study.

Solvent	Viscosity (mpa·s)	Polarity	Kinetic diameter (nm)	Total Hansen solubility parameter ($Mpa^{0.5}$)
2-propanol	2.37	4.30	0.47	24.6
ethanol	1.2	4.30	0.44	26.6
water	1	10.20	0.26	47.8
N, N-dimethylformamide	0.92	6.40	0.5	24.8
methanol	0.6	6.60	0.38	29.7
n-heptane	0.41	0.20	0.43	15.1
acetonitrile	0.37	6.20	0.34	24.3
n-hexane	0.33	0.06	0.51	14.9

Table S3 Detailed statistical percentages of different velocity distributions in both PCNN and GO channels.

Velocity of	**0-0.1**	**0.1-0.5**	**0.5-1**	**1-2.5**	**2.5-5**	**5-10**	**10-50**	**50-100**

methanol								
Percentage in PCNN	0.3533	0.0362	0.0421	0.1097	0.1426	0.1408	0.1745	0.0007
Percentage in GO	0.4047	0.0350	0.0379	0.1086	0.1321	0.1348	0.1467	0.0002

Table S4 Comparison of the filtration performance of various membranes.

Membrane	Thickness (nm)	Tested molecule	Size (nm)	Methanol permeance (LMH/bar)	Rejection (%)	Reference
PCNN/GO	60	Reactive Black	2.1×1.2	435.5	98.9	This work
TFP-DHF	61.2	Reactive Black	2.1×1.2	78	95	[8]
GO-Si2	180	Brilliant Blue	2.2×1.7	290.1	99.2	[9]
HLGO	8	Brilliant Blue	2.2×1.7	7.5	100	[10]
Tp/Bpy	2100	Brilliant Blue	2.2×1.7	108	94	[11]
Porphyrin/MPD	-	Brilliant Blue	2.2×1.7	32.5	59	[12]
M-TpTD	104000	Rose Bengal	1.5×1.2	138	84	[13]
M-TpBD	290000	Rose Bengal	1.5×1.2	106	99	[13]
PAR-BHPF/PI	20	Rose Bengal	1.5×1.2	8	99	[14]
β-CD-2.0	>500	Methyl Orange	1.2×0.7	5.5	91	[15]
TETA-TFN	-	Crystal Violet	1.4×1.3	27.8	92	[16]
rGO-TMPyP1.3	36.2	Evans Blue	3.4×1.3	13	93	[17]
SFGO-La3+	70	Acid Fuchsin	1.2×1.1	113	96	[18]
GO/BA	60	Acid Fuchsin	1.2×1.1	3.5	95	[19]

ZIF-8@GO/PEI	420	Methyl Blue	2.4×1.7	6.1	99	[20]
MXene/GO	140	Methyl Orange	1.2×0.7	50.04	97	[21]
GQD_NH_2 @PA	100	Methyl Orange	1.2×0.7	11.1	95.3	[22]
ZnS@GO	380	Evens Blue	3.4×1.3	15.8	96.8	[23]
TFC-P[6]a	8.5	Methyl Orange	1.2×0.7	8.10	96.2	[24]
TFPM-HZ/PAN	70	Congo Red	2.3×0.7	44.5	99	[25]
i-TFN	13	Rose Bengal	1.5×1.2	220.7	99.9	[26]

References

1. F. S. Guo, B. Hu, C. Yang, J. S. Zhang, Y. D. Hou and X. C. Wang, *Adv. Mater.*, 2021, **33**, 2101466.
2. X. Sui, Y. Wang, F. Liu, Z. W. Yuan, C. Wang, Y. X. Yu, K. Zhou, K. L. Goh and Y. Chen, *Matter*, 2021, **4**, 2953-2969.
3. J. J. Max and C. Chapados, *J. Phys. Chem. A*, 2004, **108**, 3324-3337.
4. J. Mohanraj, D. Durgalakshmi and R. Saravanan, *Environ. Pollut.*, 2021, **269**, 116172.
5. M. X. Wang, F. K. Ma, Z. P. Wang, D. W. Hu, X. G. Xu and X. P. Hao, *Photonics Res.*, 2018, **6**, 307-313.
6. X. P. Xin, Y. F. Xu, H. Wuliji, F. Sun, Q. D. Liu, Z. Z. Wang, T. R. Wei, X. F. Zhao, X. F. Song and L. Gao, *ACS Nano*, 2022, **17**, 657-667.
7. J. Yu, Y. Liu, X. M. Zhang, R. M. Liu, Q. Yang, S. Hu, H. O. Song, P. C. Li, A. M. Li and S. P. Zhang, *Chemosphere*, 2022, **293**, 133580.
8. D. B. Shinde, G. Sheng, X. Li, M. Ostwal, A. H. Emwas, K. W. Huang and Z. P. Lai, *J. Am. Chem. Soc.*, 2018, **140**, 14342-14349.
9. S. F. Wang, D. Mahalingam, B. Sutisna and S. P. Nunes, *J. Mater. Chem. A*, 2019, **7**, 11673-11682.
10. Q. Yang, Y. Su, C. Chi, C. T. Cherian, K. Huang, V. G. Kravets, F. C. Wang, J. C. Zhang, A. Pratt, A. N. Grigorenko, F. Guinea, A. K. Geim and R. R. Nair, *Nat. Mater.*, 2017, **16**, 1198.
11. K. Dey, M. Pal, K. C. Rout, S. Kunjattu H, A. Das, R. Mukherjee, U. K. Kharul and R. Banerjee, *J. Am. Chem. Soc.*, 2017, **139**, 13083-13091.
12. P. H. H. Duong, D. H. Anjum, K. V. Peinemann and S. P. Nunes, *J. Membr. Sci.*, 2018, **563**, 684-693.
13. S. Kandambeth, B. P. Biswal, H. D. Chaudhari, K. C. Rout, H. S. Kunjattu, S. Mitra, S. Karak, A. Das, R. Mukherjee, U. K. Kharul and R. Banerjee, *Adv. Mater.*, 2017, **29**, 1603945.
14. M. F. Jimenez-Solomon, Q. L. Song, K. E. Jelfs, M. Munoz-Ibanez and A. G. Livingston, *Nat. Mater.*, 2016, **15**, 760.
15. L. F. Villalobos, T. F. Huang and K. V. Peinemann, *Adv. Mater.*, 2017, **29**, 1606641.
16. I. Soroko and A. Livingston, *J. Membr. Sci.*, 2009, **343**, 189-198.

17. T. T. Gao, L. Huang, C. Li, G. C. Xu and G. Q. Shi, *Carbon*, 2017, **124**, 263-270.
18. L. Nie, K. Goh, Y. Wang, J. Lee, Y. J. Huang, H. E. Karahan, K. Zhou, M. D. Guiver and T. H. Bae, *Sci. Adv.*, 2020, **6**, eaaz9184.
19. T. T. Gao, H. B. Wu, L. Tao, L. T. Qu and C. Li, *J. Mater. Chem. A*, 2018, **6**, 19563-19569.
20. H. Y. Yang, N. X. Wang, L. Wang, H. X. Liu, Q. F. An and S. L. Ji, *J. Membr. Sci.*, 2018, **545**, 158-166.
21. S. C. Wei, Y. Xie, Y. D. Xing, L. C. Wang, H. Q. Ye, X. Xiong, S. Wang and K. Han, *J. Membr. Sci.*, 2019, **582**, 414-422.
22. Q. Shen, Y. Q. Lin, P. F. Zhang, J. Segawa, Y. D. Jia, T. Istirokhatun, X. Z. Cao, K. C. Guan and H. Matsuyama, *J. Membr. Sci.*, 2021, **635**, 119498.
23. N. X. Wang, H. Sun, H. Y. Yang, X. T. Li, S. L. Ji and Q. F. An, *ACS Appl. Nano. Mater.*, 2020, **3**, 5874-5880.
24. W. M. Fu, Y. Z. Huang, L. Y. Deng, J. H. Sun, S. L. Li and Y. X. Hu, *J. Membr. Sci.*, 2022, **655**, 120583.
25. X. S. Shi, Z. P. Zhang, C. C. Yin, X. Zhang, J. H. Long, Z. Zhang and Y. Wang, *Angew. Chem. Int. Ed.*, 2022, **61**, e202207559.
26. S. X. Li, Y. T. Yin, S. X. Liu, H. H. Li, B. W. Su, L. H. Han, X. L. Gao and C. J. Gao, *J. Membr. Sci.*, 2022, **662**, 120930.